

ADP-AT-98-2
Astropart. Phys., submitted

Cut-offs and pile-ups in shock acceleration spectra

R.J. Protheroe^a, Todor Stanev^b

^aDepartment of Physics and Mathematical Physics
The University of Adelaide, Adelaide, Australia 5005

^bBartol Research Institute, University of Delaware, Newark, DE 19716, USA

Abstract

We have examined cutoffs and pile-ups due to various processes in the spectra of particles produced by shock acceleration, and found that, even in the absence of energy losses, the shape of the spectrum of accelerated particles at energies well below the nominal maximum energy depends strongly on the energy dependence of the diffusion coefficient. This has implications in many areas, for example, in fitting the observed cosmic ray spectrum with models based on power-law source spectra and rigidity dependent diffusive escape from the galaxy. With continuous energy losses, prominent pile-ups may arise, and these should be included when modelling synchrotron X-ray and inverse Compton gamma-ray spectra from a shock-accelerated electron population.

We have developed a Monte Carlo/numerical technique to model the shape of the spectrum for the case of non-continuous energy losses such as inverse Compton scattering in the Klein-Nishina regime. We find that the shapes of the resulting cut-offs differ substantially from those arising from continuous processes, and we suggest that such differences could be observable through their effect on the spectrum of radiation emitted by a population of recently accelerated electrons as, for example, may exist in young supernova remnants.

PACS codes/keywords: 96.40 Cosmic rays; 96.40.De Composition, energy spectra, and interactions; 98.70.Sa Cosmic rays (including sources, origin, acceleration, and interactions)

1 Introduction

Cosmic rays with energies up to 100 TeV are thought to arise predominantly through shock acceleration by supernova remnants (SNR) in our Galaxy [1]. A fraction of the cosmic rays accelerated should interact within the supernova remnant and produce gamma-rays [2,3]. The EGRET instrument on the Compton Gamma Ray Observatory has observed gamma ray signals above 100 MeV associated with at least two supernova remnants – IC 443 and γ Cygni [4]. (It is however possible that the gamma ray emission from IC 443 is associated with a pulsar within the remnant rather than the remnant itself [5]). Further evidence for acceleration in SNR comes from the recent ASCA observation of two spatially resolved regions with non-thermal X-ray emission from SN 1006 [6]. These non-thermal X-rays are interpreted as synchrotron emission by electrons accelerated in the remnant up to energies as high as 100 TeV [7, 8]. Donea and Biermann [9] however suggest it may be bremsstrahlung from much lower energy electrons. The spectrum of synchrotron and inverse Compton emission will depend on the the electron spectrum. As we shall demonstrate in this paper the effect of a cut-off in the spectrum due to escape losses, energy losses or interactions can considerably modify the shape of the electron spectrum over several decades in energy below the nominal cut-off energy.

In this paper, we adopt a simple leaky-box model of shock acceleration based on the physical picture of acceleration at plane non-relativistic shocks. This simple model will then be used to explore the effect of cut-offs due to the finite size of the accelerator and energy-loss and interaction processes.

2 Leaky-box picture of shock acceleration

The leaky-box picture of shock acceleration [11] is based on a simple heuristic treatment of Fermi acceleration. See [12] for a simple treatment based on that in Gaisser’s book [13]. More detailed and rigorous treatments are given in several review articles [14–17].

The rate of gain of energy of relativistic particles at non-relativistic shocks is given by

$$\frac{dE}{dt} = \frac{\langle \Delta E \rangle}{t_{\text{cycle}}} \quad (1)$$

where t_{cycle} is the time for one complete cycle, i.e. from crossing the shock from upstream to downstream, diffusing back towards the shock and crossing from downstream to upstream, and finally returning to the shock, and $\langle \Delta E \rangle$ is the average energy gain per cycle.

By considering the collisionless scattering of relativistic particles by magnetic scattering centres in the upstream and downstream plasmas, one finds

$$\frac{\langle \Delta E \rangle}{E} \simeq \frac{4(R-1)}{3R} \frac{V_S}{c} \quad (2)$$

where V_s is the shock velocity, $R = u_1/u_2$ is the compression ratio, $u_1 = V_s$ and u_2 are the upstream and downstream velocities in the rest frame of the shock. For a strong shock in a monatomic gas (e.g. fully ionized plasma) $R = 4$. The acceleration rate at energy E is defined by

$$r_{\text{acc}} = \frac{1}{E} \frac{dE}{dt} \quad (3)$$

The rate of loss of accelerated particles downstream is the probability of escape per shock crossing divided by the cycle time

$$r_{\text{esc}} = \frac{\text{Prob.}(\text{escape})}{t_{\text{cycle}}}. \quad (4)$$

By considering the rate at which cosmic rays cross the shock from upstream to downstream, and rate of convection of cosmic rays downstream one obtains the probability of escape downstream per shock crossing

$$\text{Prob.}(\text{escape}) \simeq \frac{4}{R} \frac{V_S}{c} \quad (5)$$

We see immediately that the ratio of the escape rate to the acceleration rate depends on the compression ratio

$$\frac{r_{\text{esc}}}{r_{\text{acc}}} \approx \frac{3}{R-1} \quad (6)$$

and for a strong shock ($R = 4$) the two rates are equal. As we shall see below, a consequence of this is that the asymptotic spectrum of particles accelerated by a strong shock is the well-known E^{-2} power-law.

The cycle time depends on the diffusion coefficients upstream, k_1 , and downstream, k_2 , of the shock, and on the shock velocity and compression ratio and is given by

$$t_{\text{cycle}} \approx \frac{4}{c} \left(\frac{k_1}{u_1} + \frac{k_2}{u_2} \right). \quad (7)$$

The acceleration rate is then given by

$$r_{\text{acc}} \approx \frac{(R-1)u_1}{3R} \left(\frac{k_1}{u_1} + \frac{k_2}{u_2} \right)^{-1}. \quad (8)$$

Assuming the the diffusion coefficients upstream and downstream have the same power-law dependence on energy, e.g.,

$$k_1 \propto k_2 \propto E^\delta, \quad (9)$$

then the acceleration rate also has a power-law dependence

$$r_{\text{acc}} \propto E^{-\delta}. \quad (10)$$

Note that more correctly the diffusion coefficient will be a function of magnetic rigidity, ρ , which, for ultra-relativistic particles considered in this paper, is approximately equal

to E/Ze where Ze is the charge. However, in this paper since we are mainly concerned with singly charged particles we shall work in terms of E rather than rigidity.

The leaky-box acceleration model may then be considered as follows. A particle of energy E_0 is injected into the leaky box. While inside the box, the particle's energy changes at a rate $dE/dt = Er_{\text{acc}}(E)$ and that in any short time interval Δt the particle has a probability of escaping from the box given by $\Delta tr_{\text{esc}}(E)$. The energy spectrum of particles escaping from the box then approximates the spectrum of shock accelerated particles.

2.1 Energy spectrum for acceleration rate different to escape rate

Let us consider first the case of no energy losses, or losses due to any other process. N_0 particles of energy E_0 are injected at time $t = 0$, and we assume the following acceleration and escape rates:

$$r_{\text{acc}} = aE^{-\delta}, \quad (11)$$

$$r_{\text{esc}} = cE^{-\delta}. \quad (12)$$

The energy at time t is then obtained simply by integrating

$$dE/dt = aE^{(1-\delta)}, \quad (13)$$

giving

$$E(t) = (E_0^\delta + \delta at)^{1/\delta}. \quad (14)$$

The number of particles remaining inside the accelerator at time t after injection is obtained by solving

$$dN/dt = -N(t)c[E(t)]^{-\delta}. \quad (15)$$

Using Eq. 14 and integrating, one has

$$\int_{N_0}^{N(t)} N^{-1} dN = -c \int_0^t (E_0^\delta + \delta at)^{-1} dt, \quad (16)$$

giving

$$N(t) = N_0[E(t)/E_0]^{-c/a}. \quad (17)$$

Since $N_0 - N(t)$ particles have escaped from the accelerator before time t , and therefore have energies between E_0 and $E(t)$, the differential energy spectrum of particles which have escaped from the accelerator is simply given by

$$dN/dE = N_0(\Gamma - 1)(E_0)^{-1}(E/E_0)^{-\Gamma}, \quad (E > E_0) \quad (18)$$

where $\Gamma = (1 + c/a)$ is the differential spectral index. We note that for $r_{\text{esc}}(E) = r_{\text{acc}}(E)$ one obtains the standard result for acceleration at strong shocks $\Gamma = 2$.

3 Cut-off due to finite acceleration volume, etc.

Even in the absence of energy losses, acceleration usually ceases at some energy due to the finite size of the acceleration volume (e.g. when the gyroradius becomes comparable to the characteristic size of the shock), or as a result of some other process. We approximate the effect of this by introducing a constant term to the expression for the escape rate:

$$r_{\text{esc}} = cE^{-\delta} + cE_{\text{max}}^{-\delta}. \quad (19)$$

where E_{max} is defined by the above equation and will be close to the energy at which the spectrum steepens due to the constant escape term. We shall refer to E_{max} as the “maximum energy” even though some particles will be accelerated to energies above this.

Following the same procedure as for the case of a purely power-law dependence of the escape rate, we obtain the differential energy spectrum of particles escaping from the accelerator,

$$\begin{aligned} \frac{dN}{dE} &= N_0(\Gamma - 1)(E_0)^{-1}(E/E_0)^{-\Gamma} \\ &\times [1 + (E/E_{\text{max}})^\delta] \exp \left\{ -\frac{\Gamma - 1}{\delta} \left[\left(\frac{E}{E_{\text{max}}} \right)^\delta - \left(\frac{E_0}{E_{\text{max}}} \right)^\delta \right] \right\}. \quad (E > E_0) \end{aligned} \quad (20)$$

for $\delta > 0$. For $\delta = 0$ we note that from Eq. 19 $r_{\text{esc}} = (2c)$ at all energies. Thus the situation is equivalent to the case of $E_{\text{max}} \rightarrow \infty$ and the spectrum is given by Eq. 18 provided we replace c with $2c$, i.e. we must replace Γ with $\Gamma' = (2\Gamma - 1)$.

We show in Fig 1 the differential energy spectrum for Γ ranging from 1.5 to 2.5, for (a) $\delta = 1/3$, (b) $\delta = 2/3$, (c) $\delta = 1$. In Fig 2 we compare the spectra for $\Gamma = 2$ and δ ranging from $1/3$ to 1 , and note that the energy dependence of the diffusion coefficient has a profound influence on the shape of the cut-off.

Spectra such as those presented in Fig. 1 may be used to model the source spectra of high energy cosmic ray nuclei of various species if one replaces energy with magnetic rigidity, $\rho = pc/Ze \approx E/Ze$, where Z is the atomic number:

$$\begin{aligned} \frac{dN}{d\rho} &= N_0(\Gamma - 1)(\rho_0)^{-1}(\rho/\rho_0)^{-\Gamma} \\ &\times [1 + (\rho/\rho_{\text{max}})^\delta] \exp \left\{ -\frac{\Gamma - 1}{\delta} \left[\left(\frac{\rho}{\rho_{\text{max}}} \right)^\delta - \left(\frac{\rho_0}{\rho_{\text{max}}} \right)^\delta \right] \right\}. \quad (\rho > \rho_0) \end{aligned} \quad (21)$$

4 Cut-off due to E^2 energy losses

E^2 energy losses of electrons result from synchrotron radiation and inverse Compton scattering of low-energy photons in the Thomson regime. This may be treated as a continuous energy loss process. At higher energies, when the electron rest frame energy

of the emitted photon is no longer much less than the electron rest mass energy (Klein-Nishina regime of Compton scattering, or quantum synchrotron regime), the energy losses are no longer continuous and this will be discussed in Section 5.

The introduction of continuous energy losses into the problem is, in principle, straightforward and accomplished simply by modifying Eq. 13,

$$dE/dt = aE^{(1-\delta)} - bE^2. \quad (22)$$

For this case, however, the problem is easier to solve using the Green's function approach adopted by Stecker [23] when considering the ambient spectrum of cosmic ray electrons and galactic gamma-rays. Using the appropriate Green's function one can obtain the steady-state spectrum of particles inside the leaky-box accelerator, and multiplying this by the escape rate one obtains the spectrum of particles leaving the accelerator,

$$\frac{dN}{dE} = \frac{c E^{-\delta} + E_{\max}^{-\delta}}{a E^{1-\delta} - b E^2} \exp[-I(E)] \quad (23)$$

where

$$I(E) \equiv \int_{E_0}^E \frac{c E^{-\delta} + E_{\max}^{-\delta}}{a E^{1-\delta} - b E^2} dE \quad (24)$$

is given in Appendix A. The result depends on the parameters δ , Γ , E_0 , E_{cut} , E_{max} .

As a result of the energy loss by particles near the maximum energy a pile-up in the spectrum may be produced just below E_{cut} . The size of the pile-up will be determined by the relative importance of r_{acc} and r_{esc} at energies just below E_{cut} , and so should depend only on Γ and δ provided $E_0 \ll E_{\text{cut}} \ll E_{\text{max}}$. In this case, the shape of the spectrum is given by

$$\frac{dN}{dE} = N_0(\Gamma - 1)(E_0)^{-1} \left(\frac{E}{E_0}\right)^{-\Gamma} \left[1 - \left(\frac{E}{E_{\text{cut}}}\right)^{(1+\delta)}\right]^{(\Gamma-2-\delta)/(1+\delta)}. \quad (25)$$

We compare in Fig. 3 the spectra for this case for $\delta = 1/3$, $2/3$ and 1 , and for $\Gamma = 1.5$, 2 , and 2.5 , and note that the pile-ups are higher for flatter spectra, and that for steep spectra the pile-up may be absent or the spectrum may steepen before the cut-off if δ is small. The effect of synchrotron losses on multiple diffusive shock acceleration have been considered by Melrose and Crouch [24], and similar effects were found.

For the case where E_{cut} is comparable to or not much less than E_{max} we show in Fig 4 the differential energy spectrum for $\Gamma = 2$ for (a) $\delta = 1/3$, (b) $\delta = 2/3$, (c) $\delta = 1$, and in each case we show results for $E_{\text{cut}}/E_{\text{max}}$ ranging from 10^{-5} to 10^1 . Figs. 4(a)—(c) are identical in the sense that they are all for $\Gamma = 2$ and show synchrotron cutoffs at 1 , $1/10$, ... 10^{-5} of E_{max} . The only difference is in the energy dependence of the diffusion coefficient. In Fig. 4(c), for $\delta = 1$, the shape of the pile-up is independent of E_{cut} for $E_{\text{cut}} \leq 0.1E_{\text{max}}$. In contrast, in Fig. 4(a), for $\delta = 1/3$, the size of the pile-up decreases

with increasing $E_{\text{cut}}/E_{\text{max}}$, and so does not depend simply on Γ and δ . This is because the constant escape term gives rise to a steepening in the spectrum, and thus from Fig. 3 we expect a smaller synchrotron pile-up, or even a steepening. For example, note that in Fig. 4(a), for $\delta = 1/3$ the the spectrum in the absence of synchrotron losses steepens at significantly lower energies (due to the constant leakage term) than for the case of $\delta = 1$, and at $E = 10^{-2}E_{\text{max}}$ has a differential index of ~ 2.2 . We plot in Fig. 4(d) results generated for $\Gamma = 2.2$ and $\delta = 1/3$ and note that the size of the pile-up for $E_{\text{cut}} \ll E_{\text{max}}$ is similar to the case for $\Gamma = 2$, $\delta = 1/3$, and $E = 10^{-2}E_{\text{max}}$.

5 Cut-off due to inverse Compton losses on the 2.7 K background

In this section, we discuss the acceleration of electrons in the presence of a blackbody radiation field. Such a scenario is important in many areas of high energy astrophysics. For example, one may have acceleration of electrons in active galactic nuclei being responsible for radio, optical, X-ray, and gamma-ray emission, and this acceleration takes place in the presence of an intense radiation field, e.g. from the accretion disk.

We choose as our example, the case where the cosmic microwave background radiation is the dominant radiation field. Such a situation would occur during 1st order Fermi acceleration of cosmic ray electrons in our Galaxy at a shock in the interstellar medium due to a young supernova remnant.

5.1 Times scales for losses and acceleration

The energy loss rate is given by

$$\frac{dE}{dt} = -\frac{4}{3}\sigma_T c U \gamma^2 \quad (26)$$

where σ_T is the Thomson cross section, γ is the electron's Lorentz factor, and $U = B^2/8\pi$ for synchrotron losses and U is the energy density of the radiation field for inverse Compton losses in the Thomson regime ($U_{\text{rad}} = aT^4$ for blackbody radiation). Thus, at low energies, the time scale for energy loss of an electron by synchrotron losses is given by

$$\frac{E}{-dE/dt} = 1.3 \times 10^{10} \left(\frac{E}{1 \text{ GeV}}\right)^{-1} \left(\frac{B}{1 \mu\text{G}}\right)^{-2} \text{ years}, \quad (27)$$

while that for IC scattering is given by

$$\frac{E}{-dE/dt} = 1.3 \times 10^9 \left(\frac{E}{1 \text{ GeV}}\right)^{-1} \left(\frac{T}{2.735}\right)^{-4} \text{ years}. \quad (28)$$

The energy loss time scale for synchrotron losses is shown in Figs. 5(a)—(c) for B ranging from 10^{-11} G to 10^{-5} G by the dotted lines.

For electrons with energies above $\sim 3 \times 10^4$ GeV energy losses during inverse Compton scattering on the microwave background photons are no longer continuous. The Klein-Nishina cross section must be used, and in each interaction the electron loses a substantial fraction of its energy. Monte Carlo simulations using the differential Klein-Nishina cross section have been performed and the mean energy loss per interaction $\langle \Delta E \rangle$ has been calculated as a function of the electron energy. One can thus obtain an effective energy-loss time scale, $Et_{\text{int}}/\langle \Delta E \rangle$, where t_{int} is the mean interaction time. See [25–28] for discussion of Monte Carlo calculations of inverse Compton scattering. The energy loss time scale and the interaction time for IC losses are shown in Figs. 5(a)–(c) by the thick solid curves, and dashed curves labelled ‘IC’ (the thin solid curves, and dashed curves labelled ‘TPP’ give the energy loss time scale and the interaction time for triplet pair production; see e.g. [29]).

During acceleration, the cut-off energy (and the loss process responsible) will depend on the strength of the magnetic field and the acceleration rate. The acceleration rate is inversely proportional to the diffusion coefficient (see Eq. 7), and so the highest acceleration rate is achieved with the lowest diffusion coefficient.

The diffusion coefficients required k_1 and k_2 are the coefficients for diffusion parallel to the shock normal. The diffusion coefficient along the magnetic field direction is some factor η times the minimum diffusion coefficient, known as the Bohm diffusion coefficient,

$$k_{\parallel} = \eta \frac{1}{3} R_g c \quad (29)$$

where R_g is the gyroradius, and $\eta > 1$.

Parallel shocks are defined such that the shock normal is parallel to the magnetic field ($\vec{B} \parallel \vec{u}_1$). In this case, making the approximation that $k_1 = k_2 = k_{\parallel}$, $R = 4$, and $B_1 = B_2$ one obtains

$$r_{\text{acc}}^{\parallel} \approx \frac{3\beta_1^2}{20\eta} \omega_g \quad (30)$$

where $\beta_1 = u_1/c$ and $\omega_g = c/R_g$. For a shock speed of $u_1 = 0.1c$ and $\eta = 10$ one obtains an acceleration rate

$$r_{\text{acc}}^{\parallel} \approx 1.5 \times 10^{-4} \omega_g. \quad (31)$$

For the oblique case, the angle between the magnetic field direction and the shock normal is different in the upstream and downstream regions, and the direction of the plasma flow also changes at the shock. The diffusion coefficient in the direction at angle θ to the magnetic field direction is given by

$$k = k_{\parallel} \cos^2 \theta + k_{\perp} \sin^2 \theta \quad (32)$$

where k_{\perp} is the diffusion coefficient perpendicular to the magnetic field. Jokipii [22] shows that

$$k_{\perp} \approx \frac{k_{\parallel}}{1 + \eta^2} \quad (33)$$

provided that η is not too large (values in the range up to 10 appear appropriate).

In the case of acceleration at perpendicular shocks, Jokipii [22] has shown that acceleration can be much faster than for the parallel case. Using k_{\perp} and $B_2 \approx 4B_1$ and one obtains

$$r_{\text{acc}}^{\perp} \approx \frac{3\beta_1^2 \eta}{8} \omega_g. \quad (34)$$

For a shock speed of $u_1 = 0.1c$ and $\eta = 10$ one obtains an acceleration rate of

$$r_{\text{acc}}^{\perp} \approx 0.04\omega_g. \quad (35)$$

Generally, for stochastic particle acceleration by electric fields induced by motion of magnetic fields the acceleration rate is given by

$$r_{\text{acc}} = \xi(E)\omega_g \approx 0.01\xi(E) \left(\frac{E}{1 \text{ GeV}} \right)^{-1} \left(\frac{B}{1 \mu\text{G}} \right) \text{ s} \quad (36)$$

where $\xi(E) \leq 1$ and depends on the acceleration mechanism; constant values of ξ ranging from 1.5×10^{-4} to 0.04 might be achieved by first order Fermi acceleration with Bohm diffusion ($k \propto E$, i.e. $\delta = 1$).

We show in Fig. 5(a), along with the energy loss time scales for IC and synchrotron losses, the acceleration time scale for $\delta = 1$ (Bohm diffusion) for ranges of ξB which are probably appropriate for supernova shocks. Comparing the energy loss time scale for IC and synchrotron loss we see that if $B > 3 \mu\text{G}$ the cut off will be determined by synchrotron losses irrespective of the acceleration rate. Conversely, if $B < 3 \mu\text{G}$ the cut off will be determined by IC provided the acceleration rate is low such that the acceleration time curve intersects the IC loss curve in the Thomson regime. However, if the magnetic field is less than $\sim 1 \mu\text{G}$ and ξB is in the range 10^{-8} to $10^{-6} \mu\text{G}$, the cut-off in the spectrum of accelerated electrons will be determined by IC scattering in the Klein-Nishina regime. If the magnetic field were less than $0.1 \mu\text{G}$, the range of ξB would be extended up to $10^{-5} \mu\text{G}$, but for $\xi B > 1.4 \times 10^{-5} \mu\text{G}$ the cut off will be determined by synchrotron losses. If the cut off is determined by IC in the K-N regime, the shape of the cut-off would be different from that calculated for the case of E^2 energy losses, and one would need to take account properly of inverse Compton collisions in the Klein-Nishina regime. The spectrum of synchrotron radiation and inverse Compton gamma-rays would also depend on the details of the electron spectrum cut-off and would therefore differ from the E^2 energy loss case.

In Fig. 5(b) we show acceleration time scales that would apply if we used the diffusion coefficient inferred from a comparison of cosmic ray data with propagation model calculations [30], $k = 2.5 \times 10^{28} (E/3 \text{ GeV})^{0.6} \text{ cm}^2 \text{ s}^{-1}$, and shock velocities ranging from $0.01c$ to $0.1c$. In this case, the cut-off energy would probably be determined by IC in the Thomson regime or by synchrotron losses.

In Fig. 5(c) we show acceleration time scales that would arise in the case of a Kolmogorov spectrum of turbulence. A range of acceleration times (chain lines) are shown

for the purpose of illustration only. The diffusion coefficient can never be lower than the minimum (Bohm) diffusion coefficient, and so with increasing energy these curves would violate the Bohm limit. Thus the curves shown above $\sim 10^4$ GeV are unrealistic for acceleration at supernova remnant shocks in our Galaxy with typical galactic magnetic fields. The curves in Fig. 5(c) should bend upwards and smoothly join an appropriate curve from Fig. 5(a). However, with an acceleration rate such as given by the middle curve, the cut-off energy determined by IC scattering would not be precisely determined, and could be anywhere between 3×10^5 and 3×10^7 GeV, and this would result in an interesting spectral shape. While this scenario does not apply at galactic supernova shocks, it may well apply in other astrophysical environments where shocks are present and different radiation fields exist.

6 Monte Carlo Simulation

A set of programs was constructed that simulates the particle acceleration in the leaky box acceleration model using the Monte Carlo method. In the simulation, a particle is injected with energy E_0 and the acceleration and escape are simulated for a given E_{\max} value and specific energy dependence of the diffusion coefficient. After the injection with energy E_0 the development of the electron energy spectrum is followed in time steps Δt . At every step the particles gain energy $\Delta t(dE/dt)$. Δt was chosen to be small, 1/100 of the escape time at E_0 . The spectrum of the escaping particles is calculated by weighting the particle energy after each step i by $P_{\text{esc}}^i \times P^{i-1}$, where P^{i-1} is the probability that the particle has remained in the accelerator region for $i - 1$ time steps. P_{esc} is calculated as a function of the particle energy for the chosen energy dependence of the diffusion coefficient with a constant $P_{\text{esc}}(E_{\max})$ added to simulate a smooth cutoff in the escaping particle spectrum. The maximum acceleration time was calculated so that particles could have reached energy of $10E_{\max}$ in the absence of the constant term in the escape probability.

The advantage of the Monte Carlo/numerical approach is that it is easily adapted to calculate the escaping electron spectrum for both continuous energy losses (e.g. synchrotron or IC in the Thomson regime) and non-continuous energy losses (e.g. IC in the KN regime). We next present results obtained by the numerical/Monte Carlo technique produced in a series of runs made including synchrotron energy loss. The energy loss was calculated at every Δt and subtracted from the energy gain. The magnetic field value necessary for generating a cutoff at 1, 1/10, 1/100, 1/1000, and 1/10000 of E_{\max} was calculated keeping all ‘acceleration’ parameters as before. The program was tested for the same parameters used in the analytical/numerical technique described earlier, and the agreement was found to be excellent. We show, for example, in Fig. 6 the spectrum of accelerated particles in the presence of synchrotron losses for $\delta = 1/3$ obtained using the Monte Carlo method and compare this with the analytic results obtained previously.

6.1 Comparison of cutoffs due to synchrotron and IC energy loss

Next we used the same procedure to simulate non-continuous inverse Compton energy loss. IC in the Klein-Nishina regime was incorporated as follows: for every time step, Δt , the IC interaction time was sampled from an exponential distribution with mean interaction time, t_{int} as a function of the electron energy (given by the long-dashed curve in Fig. 5). If the sampled interaction time was less than Δt , an IC collision was simulated by the Monte Carlo method and the electron energy loss was subtracted from the energy gain due to acceleration in the time step. E_{max} was set to 10^6 GeV to enable us to study the non-continuous energy loss in the Klein-Nishina regime. All acceleration parameters were adjusted to produce an IC energy loss time equal to the acceleration time at the same E_{cut} values as in the synchrotron case above.

Figs. 7(a) and 7(b) show the electron spectrum in the presence of IC energy loss for the case of $\delta = 1/3$ and $\delta = 1$ respectively. Note that for $E_{\text{cut}} = 1000$ GeV, where IC is in the Thompson regime and the energy loss is quasi-continuous, the picture is similar to that in the synchrotron case (Figs. 4(a) and (c)). For $E_{\text{cut}} = 10^6$ GeV, where IC is in the Klein-Nishina regime, the shape of the cutoff is qualitatively different and much smoother.

Fig. 7(b) is the version of Fig. 7(a) for the case of diffusion coefficient $\propto E$. In the case of $E^{1/3}$ energy dependence of the diffusion coefficient the pile-ups are much smaller and almost do not exist for $E_{\text{cut}}/E_{\text{max}}$ greater than 10^{-3} . Pile-ups are significantly more pronounced when the diffusion coefficient is proportional to E . The shape of these pile-ups, especially for IC losses in the Klein-Nishina regime, is very different from the synchrotron loss case (Figs. 4(a) and (c)).

Fig. 8 compares the cutoffs due to synchrotron energy loss to those of IC energy loss on a linear scale. We show this comparison with a histogram because histograms are a better presentation of the Monte Carlo approach than smooth curves.

The dotted histogram in Fig. 8 shows the cut-offs and pile-ups that are produced by IC energy loss. For $E_{\text{cut}}/E_{\text{max}}$ of 10^{-3} the shape of the pile-up in the spectrum of accelerated electrons is not very different from the synchrotron loss case. The reason is, of course, that the IC energy loss of 1000 GeV electrons in the Thompson regime is almost continuous, very similar to the synchrotron loss. For higher ratios, when the IC collisions move deeper and deeper in the Klein-Nishina regime and the energy loss becomes a significant fraction of the total electron energy, pile-ups become very wide, while for $E_{\text{cut}} = E_{\text{max}}$ there is no pile-up. It is replaced by a spectral cut-off which is very different from the cut-offs due to synchrotron loss or to escape from the shock.

7 Conclusion

We have derived the shape of the spectrum of particles produced by 1st order Fermi acceleration near the maximum or cut-off energy when the maximum energy is caused

by a constant escape rate term. We found that, even in the absence of energy losses, the shape of the spectrum of accelerated particles at energies well below the nominal maximum energy depends strongly on the energy dependence of the diffusion coefficient. This has implications in many areas, for example, in fitting the shape of the observed cosmic ray spectrum in the region of the “knee” with model spectra based on power-law acceleration spectra and rigidity dependent diffusive escape from the galaxy.

In the case where the cut-off is due to continuous energy losses a prominent pile-up may occur just below the cut-off energy defined as the energy at which the total rate of change of energy is zero, and the spectrum cuts off sharply at this energy.

We have developed a Monte Carlo/numerical technique to model cut-offs caused by non-continuous energy losses (i.e. interactions in which the particle being accelerated loses a substantial fraction of its energy). The Monte Carlo technique is tested by comparisons with the analytic calculations in cases where possible. Using numerical calculations we find that in the case of discrete energy loss the pile-up, if present, is less pronounced, and the cut-off is smoother with particle energies extending beyond the cut-off energy. This may well have observational consequences as it will affect the spectrum of synchrotron radiation and inverse Compton radiation.

Further applications of this technique will compare the radiation spectra due to synchrotron radiation and to IC energy loss by the accelerated electrons and to those that escape from the shock in more realistic astrophysical environments, related to the environments in different galactic supernova remnants. The technique developed can also be used to study the shape of the energy spectra of protons accelerated to ultra high energy in the presence of energy loss, such as pair production and photoproduction on the ambient photon fields. In addition, the Monte Carlo technique developed can be used for studies of the shape of the energy spectra of the accelerated particles in the presence of energy loss in more complicated acceleration models, including non linear shock models where the effective compression ratio is a function of the rigidity of the accelerated particles. We also intend to apply this method to study the shape of the proton spectra accelerated to ultra high energy in the presence of pair production and photoproduction losses in interactions on the ambient photon fields.

Acknowledgments

We thank Troy Porter for helpful suggestions. T.S. thanks the University of Adelaide for hospitality during his visit which was funded partly by the International Visitor Program of the Special Research centre for Theoretical Astrophysics, University of Sydney, and partly from an Australian Research Council grant to R.J.P. The research of R.J.P. is funded by the Australian Research Council. The research of T.S. is funded in part by NASA grant NAG5-5106.

References

- [1] Lagage, P.O., and Cesarsky, C.J., *Astron. Astrophys.* **118** (1983) 223
- [2] Drury, L.O'C., Aharonian, F.A., and Völk, H.J., *Astron. Astrophys.* **287** (1994) 959.
- [3] Gaisser, T.K., Protheroe, R.J., and Stanev, T., *Astrophys. J.* **79** (1997) 2616.
- [4] Esposito, J.A., Hunter, S.D., Kanbach, G., and Sreekumar, P., *Astrophys. J.* **461** (1996) 820.
- [5] Brazier, K.T.S., Kanbach, G., Carraminana, A., Guichard, J., and Merck, M., *Mon. Not. R. Astr. Soc.*, **281** (1996) 1033.
- [6] Koyama, K., Petre, R., Gotthelf, E.V., Hwang, U., Matsuura, M., Ozaki, M., and Holt, S.S., *Nature* **378** (1995) 255.
- [7] Reynolds, S.P., *Astrophys. J. Lett.* **459** (1996) L13.
- [8] Mastichiadis, A., *Astron. Astrophys.*, **305** (1996) 53.
- [9] Donea, A.C., and Biermann, P.L., *Astron. Astrophys.* **316** 43 (1996).
- [10] Markiewicz W.J., Drury L. O'C., and Volk H.J., *Astron. Astrophys.* **236** (1990) 487.
- [11] Szabo, A.P., and Protheroe, R.J., *Astropart. Phys.*, **2** (1994) 375.
- [12] Protheroe, R.J., in *Towards the Millennium in Astrophysics: Problems and Prospects*, Erice 1996, eds. M.M. Shapiro and J.P. Wefel (World Scientific, Singapore), in press (1998). astro-ph/9612212
- [13] Gaisser, T.K., *Cosmic Rays and Particle Physics*, (Cambridge University Press, Cambridge, 1990).
- [14] Drury, L.O'C., *Space Sci. Rev.* **36** (1983) 57.
- [15] Blandford, R., and Eichler, D., *Phys. Rep.* **154** (1987) 1.
- [16] Berezhko, E.G., and Krymski, G.F., *Usp. Fiz. Nauk* **154** (1988) 49.
- [17] Jones, F.C., and Ellison, D.C., *Space Sci. Rev.* **58** (1991) 259.
- [18] Axford, W.I., Lear, E., and Skadron, G., *Proc. 15th Int. Cosmic Ray Conf., Ploudiv*, **11** (1977) 132.
- [19] Krymsky, G.F., *Dokl. Akad. Nauk. SSSR*, **243** (1977) 1306.
- [20] Bell, A.R., *Mon. Not. R. Astr. Soc.*, **182** (1978) 443.

- [21] Blandford, R.D., and Ostriker, J.P., *Astrophys. J. Lett.* **221** (1978) L29.
- [22] Jokipii, J.R., *Astrophys. J.* **313** (1987) 842.
- [23] Stecker, F.W., “Cosmic Gamma Rays” (Baltimore: Mono Book Co., 1971) p. 133.
- [24] Melrose, D.B., and Crouch, A.D., *Publ. Astron. Soc. Aust.* **14** (1997) 251.
- [25] Protheroe, R.J., *Mon. Not. R. Astron. Soc.* **221** (1986) 769.
- [26] Protheroe, R.J., *Mon. Not. R. Astr. Soc.* **246** (1990) 628.
- [27] Protheroe, R.J., Mastichiadis A. and Dermer C.D. *Astroparticle Phys.* **1** (1992) 113.
- [28] Protheroe, R.J., and Stanev, T.S., *Mon. Not. R. Astron. Soc.* **264** (1993) 191.
- [29] Mastichiadis, A., Szabo, A.P., and Protheroe, R.J., *Mon. Not. R. Astron. Soc.* **266** (1994) 910.
- [30] Porter, T.A., and Protheroe, R.J., *J. Phys. G: Nucl. Part. Phys.*, **23** (1997) 1765.

Appendix A

Using the Green's function (e.g. [23]) for the “leaky-box model” of cosmic ray propagation, more properly called the homogeneous model, one can find the steady-state solution for the energy spectrum of particles inside the leaky-box

$$\frac{dN_{\text{in}}}{dE} = \frac{N_0}{R(E)} \exp \left\{ - \int_{E_0}^E \frac{dE'}{\tau(E')R(E')} \right\} \quad (37)$$

where $R(E)$ is the rate of energy gain and $\tau(E)$ is the escape time. We can use this in the present case of the leaky box acceleration model with, $R(E) = (aE^{1-\delta} + bE^2)$ and $\tau(E) = (cE^{-\delta} + cE_{\text{max}}^{-\delta})^{-1}$. We require the spectrum of accelerated particles, i.e. those escaping from the leaky-box, and this is simply dN_{in}/dE divided by the escape time $\tau(E)$:

$$\frac{dN}{dE} = \frac{cE^{-\delta} + cE_{\text{max}}^{-\delta}}{aE^{1-\delta} - bE^2} N_0 \exp[-I(E)] \quad (38)$$

where

$$\begin{aligned} I(E) &\equiv \int_{E_0}^E \frac{cE^{-\delta} + cE_{\text{max}}^{-\delta}}{aE^{1-\delta} - bE^2} dE, \\ &= \left[\left(\frac{c}{a\delta} \right) \left(\frac{E}{E_{\text{max}}} \right)^\delta {}_2F_1 \left(\frac{\delta}{1+\delta}, 1, 1 + \frac{\delta}{1+\delta}, \frac{bE^{1+\delta}}{a} \right) \right. \\ &\quad \left. - \frac{c}{a(1+\delta)} \ln \left(b - \frac{a}{E^{1+\delta}} \right) \right]_{E_0}^E, \end{aligned} \quad (39)$$

$$\quad (40)$$

and ${}_2F_1$ is the hypergeometric function.

Substituting the integration limits, and using $\Gamma = (1 + c/a)$, and $E_{\text{cut}} = (a/b)^{1/(1+\delta)}$ we obtain

$$\frac{dN}{dE} = \frac{(\Gamma - 1)(E^{-\delta} + E_{\text{max}}^{-\delta})}{E^{1-\delta} - E^2 E_{\text{cut}}^{-(1+\delta)}} N_0 \exp[-I(E)] \quad (41)$$

where

$$\begin{aligned} I(E) &= \left(\frac{\Gamma - 1}{\delta} \right) \left(\frac{E}{E_{\text{max}}} \right)^\delta \left\{ {}_2F_1 \left[\frac{\delta}{1+\delta}, 1, 1 + \frac{\delta}{1+\delta}, \left(\frac{E}{E_{\text{cut}}} \right)^{1+\delta} \right] \right. \\ &\quad \left. - {}_2F_1 \left[\frac{\delta}{1+\delta}, 1, 1 + \frac{\delta}{1+\delta}, \left(\frac{E_0}{E_{\text{cut}}} \right)^{1+\delta} \right] \right\} \\ &\quad - \left(\frac{\Gamma - 1}{1+\delta} \right) \ln \left(\frac{E_{\text{cut}}^{-(1+\delta)} - E^{-(1+\delta)}}{E_{\text{cut}}^{-(1+\delta)} - E_0^{-(1+\delta)}} \right). \end{aligned} \quad (42)$$

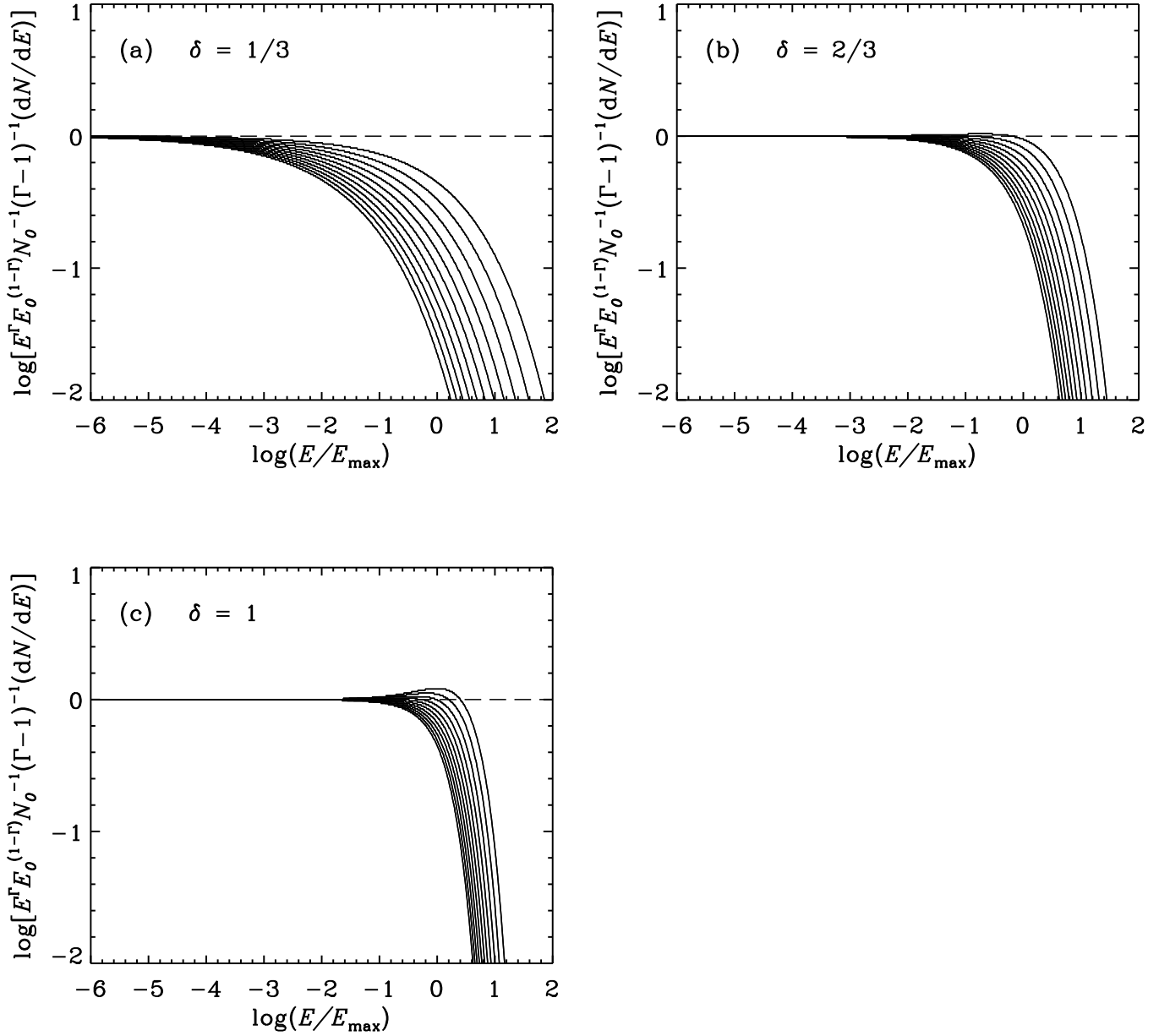


Figure 1: Differential energy spectrum for (a) $\delta = 1/3$, (b) $\delta = 2/3$, (c) $\delta = 1$. In each case we show results for $\Gamma = 1.5$ (highest curve), 1.6, 1.7, ..., 2.5 (lowest curve).

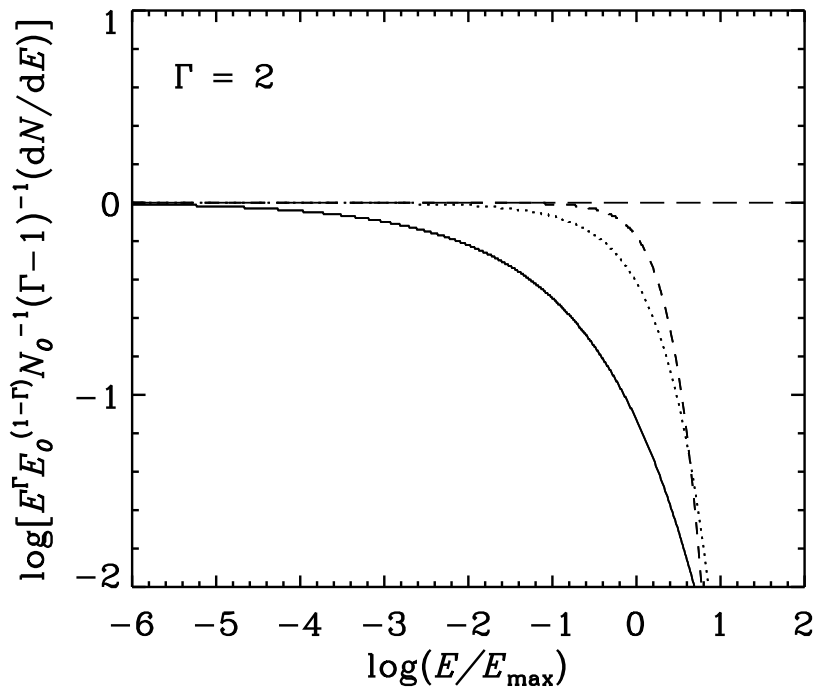


Figure 2: Differential energy spectrum for $\Gamma = 2$ and $\delta = 1/3$ (solid curve), $2/3$ (dotted curve) and 1 (dashed curve).

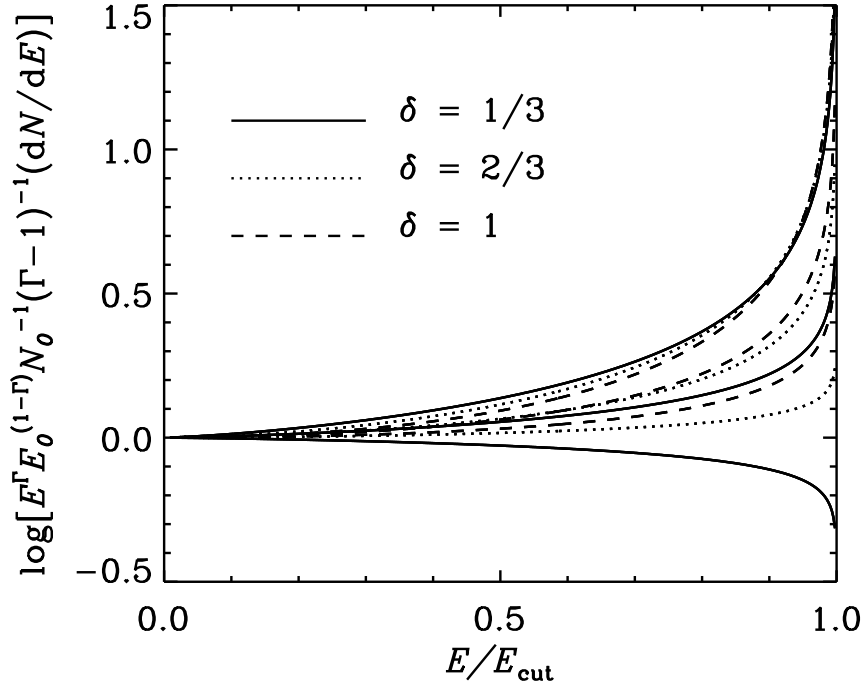


Figure 3: Differential energy spectra for $E_0 \ll E_{\text{cut}} \ll E_{\text{max}}$ for $\delta = 1/3$ (solid curves), $2/3$ (dotted curves) and 1 (dashed curves), and $\Gamma = 1.5$ (upper curves), 2.0 (middle curves) and 2.5 (lower curves).

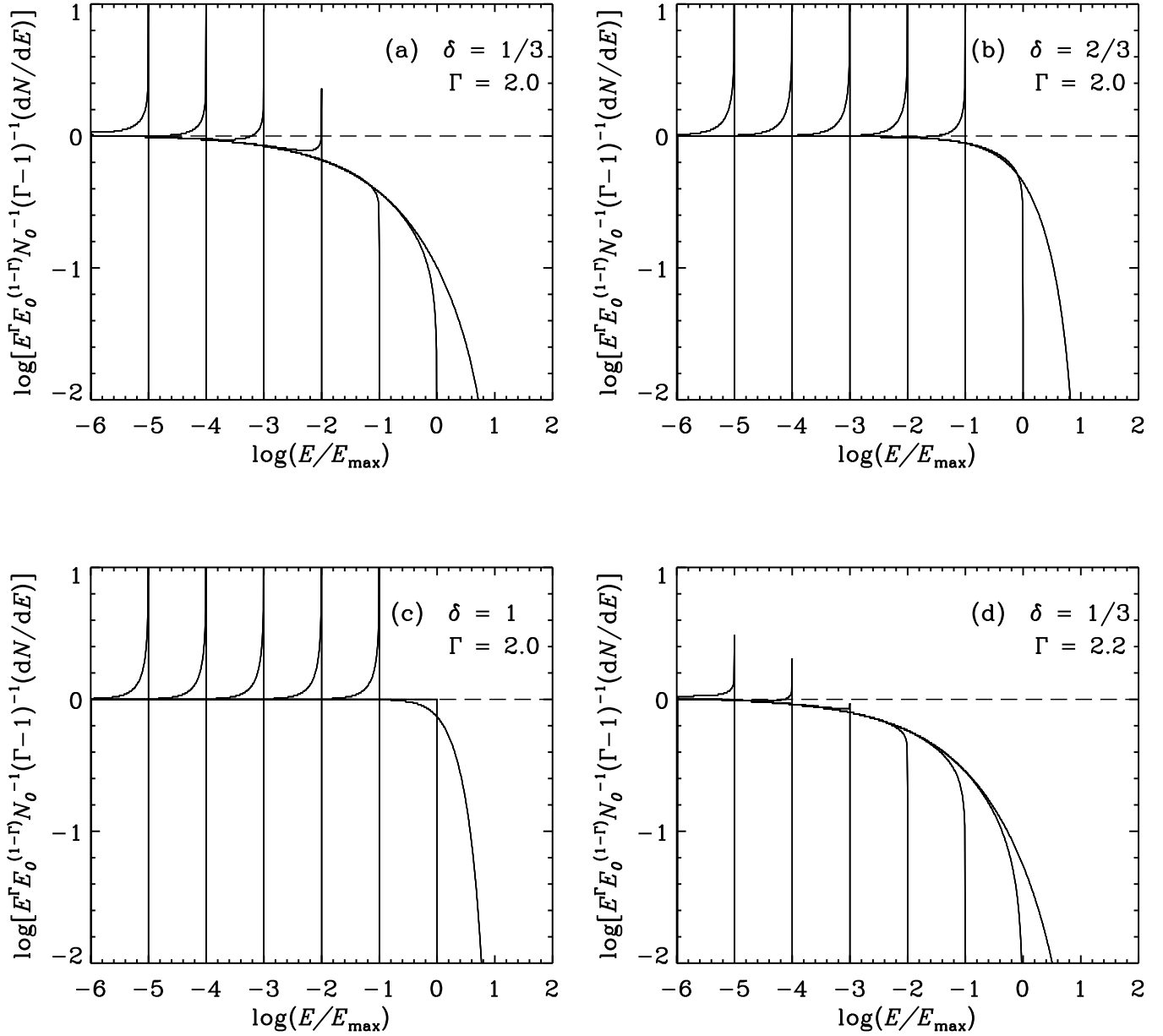


Figure 4: Differential energy spectrum for $\Gamma = 2$ for (a) $\delta = 1/3$, (b) $\delta = 2/3$, (c) $\delta = 1$, and (d) for $\Gamma = 2.2$ and $\delta = 1/3$. In each case we show results for $E_{\text{cut}}/E_{\text{max}} = 10^{-5}$ (leftmost curve), $10^{-4}, \dots, 10^1$ (rightmost curve).

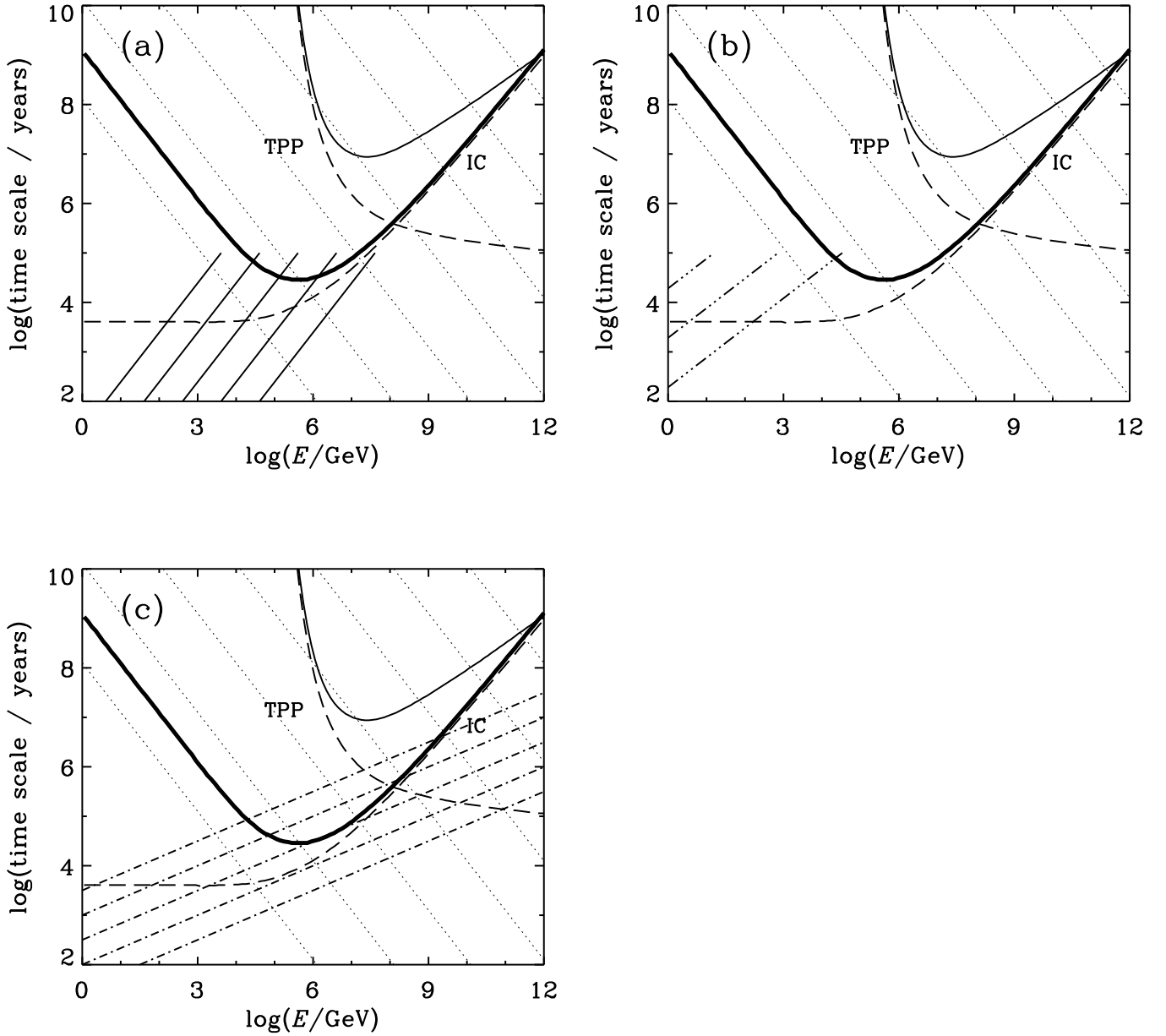


Figure 5: The energy loss time scale for synchrotron losses are shown by thin dotted lines for $B = 10 \mu\text{G}$ (lowest line), $1 \mu\text{G}$, $0.1 \mu\text{G}$, ... 10^{-11}G (highest line). For IC, the energy loss time scale (thick solid line labeled IC) and mean interaction time (dashed line labeled IC) are shown; the corresponding curves labelled TPP are for triplet pair production. Acceleration time scales are shown for: (a) $\delta = 1$ (Bohm diffusion) with $\xi B = 1.4 \times 10^{-9} \mu\text{G}$ (leftmost solid line), 1.4×10^{-8} , ... $1.4 \times 10^{-5} \mu\text{G}$ (rightmost solid line); (b) $\delta = 0.6$ which has been suggested for the propagation of Galactic cosmic rays and $u_1 = 0.1c$ (lowest chain line), $0.03c$, and $0.01c$ (highest chain line); (c) $\delta = 1/3$ which would arise in the case of a Kolmogorov spectrum of turbulence – a range of acceleration times (chain lines) are shown for the purpose of illustration.

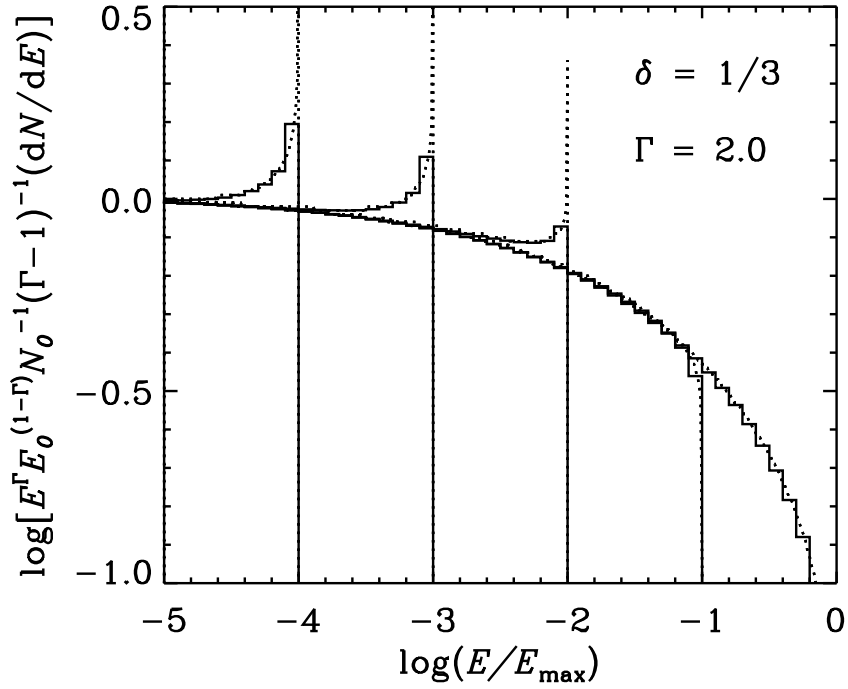


Figure 6: Spectrum of accelerated electrons obtained using the Monte Carlo technique (histograms) compared with the analytic result from Fig. 4(a) for $E_{\max} = 10^6$ GeV and cutoff due to synchrotron energy loss of 1, 1/10, 1/100, 1/1000, and 1/10000 E_{\max} . The diffusion coefficient is proportional to $E^{1/3}$.

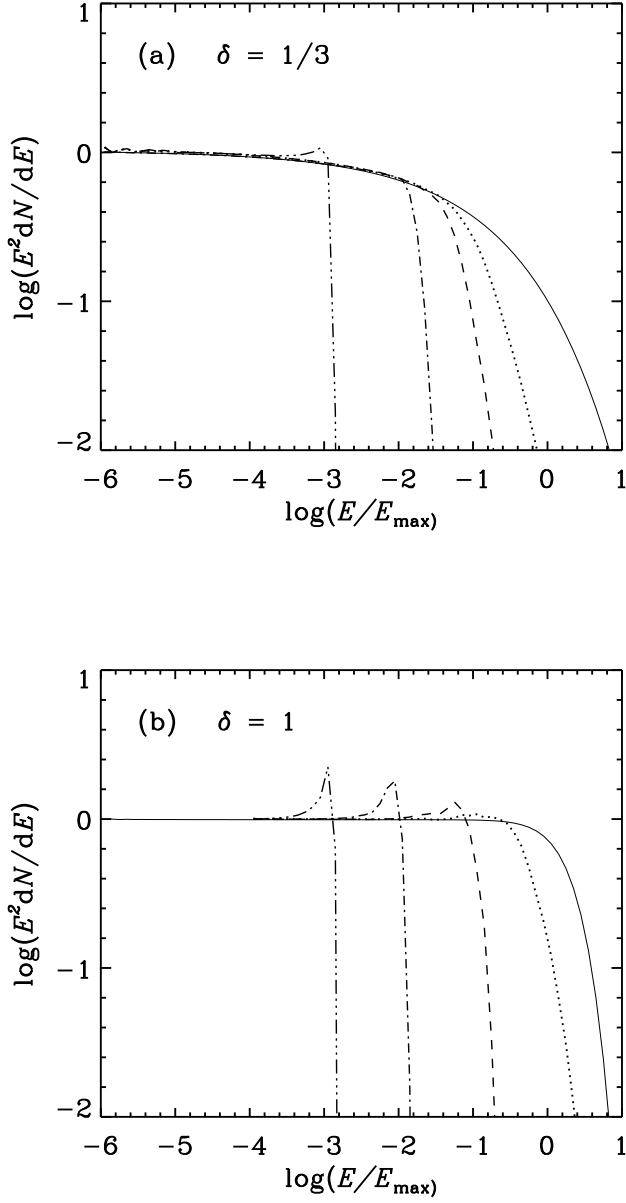


Figure 7: Spectrum of accelerated electrons for $E_{\max} = 10^6$ GeV and cutoff due to IC energy loss at 1, 1/10, 1/100, and 1/1000 E_{\max} . The diffusion coefficient is proportional to (a) $E^{1/3}$, (b) E .

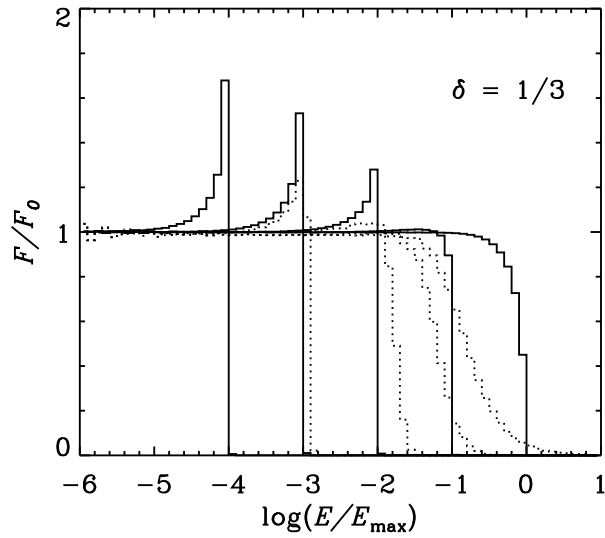


Figure 8: Spectrum of accelerated electrons for $E_{\max} = 10^6$ GeV and cutoffs due to synchrotron (solid histogram) and IC energy loss (dotted histogram). Spectrum, divided by that for no IC loss, is shown on a linear scale to emphasize the cutoffs. The diffusion coefficient is proportional to $E^{1/3}$ (F/F_0 represents the ratio of the spectrum calculated with energy losses to the spectrum calculated without energy losses).